Direct observations of the onset of continuous edge instability limiting the pedestal growth between ELMs

A. Diallo[1], J.W.Hughes[2], M.Greenwald[2], J.Walk[2], C.Theiler[2], B.LaBombard[2], M.L.Reinke[2], T.Golfinopoulos[2], E.Davis[2], S-G.Baek[2], L.Delgado-Aparicio[1], A.Hubbard[2], J.Terry[2], A.White[2], and the Alcator C-Mod team.

[1] *Princeton Plasma Physics Laboratory, Princeton, USA*

[2] *Plasma Science and Fusion Center, MIT, Cambridge, MA, USA*

Introduction

Improvement in global confinement and fusion performance are found to be correlated with the pressure at the top of the edge barrier ("pedestal height") both in experiments and theory. Performance predictions for future devices rely on experimental validations of the hypothesis in the predictive models. To date, the leading model for pedestal structure prediction is EPED [1]. This model uses both the peeling ballooning theory to limit the pedestal height and relies on the onset of the kinetic ballooning mode (KBM) to constrain the pedestal gradient. Here, we test the KBM hypothesis during the inter-edge-localized-mode (ELM) phase by investigating the onset of the KBM for providing the necessary transport limiting the pedestal gradient evolution.

Global and edge profile characterization

This section provides the discharge characteristics, including details on the access to ELMy H-mode in Alcator C-Mod tokamak. This compact tokamak operates with major radius $R = 67$ cm and minor radius $a = 21$ cm, magnetic field strength ranging from 2.6 T to 8.0 T, and high densities ($< 10^{21}$ m^{-3}). The H-mode discharges presented here were induced using auxiliary heating from Ion Cyclotron Range of Frequency (ICRF) minority heating[2].

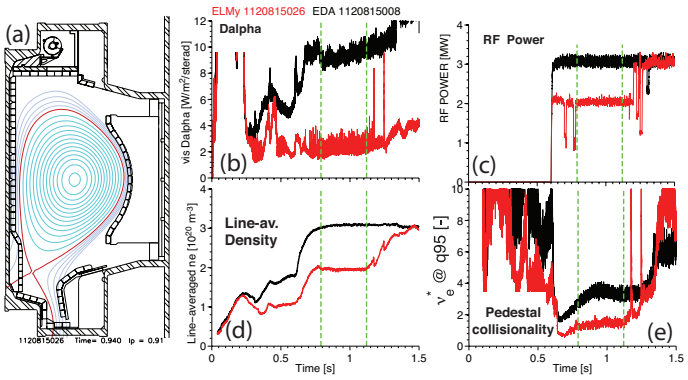

Figure 1: (color online) Experimental characterization of ELMy and EDA H-mode: (a) Magnetic flux contours of discharges. (b) - (e) Time history of EDA (black) and ELMy(red) discharges for comparison.

The investigation of the inter-ELM fluctuations responsible for limiting the pedestal parameters requires reliable access to ELMy H-mode discharges. These discharges are

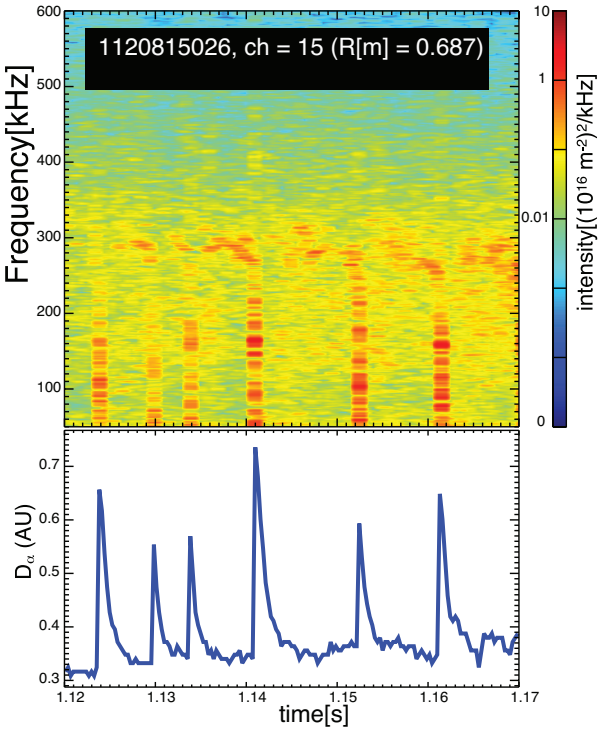

Figure 2: (color online)Spectrogram for edge channel from the PCI diagnostics. Bottom panel shows the D_α trace indicating ELMs.

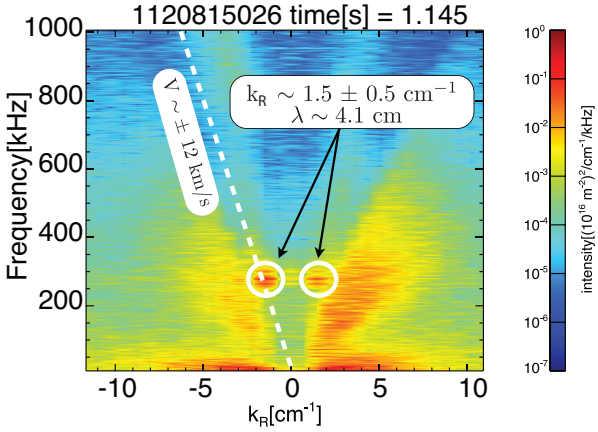

Figure 3: (color online) Frequency and wavenumber spectrum at t = 1.145s indicating two coherent peaks

typically achieved when Alcator C-Mod is operated with an equilibrium shape consisting of a low elongation ($\kappa \sim 1.4 - 1.5$) and high lower triangularity ($\delta_l \sim 0.8$) (see Ref. [3] for details). In addition, the outer-divertor leg is steered to the more closed flat plate of the divertor floor (see fig. 1(a)). Such divertor configuration, in combination with a reduced fueling yields lower than usual pedestal collisionality ($\nu^*_{ped} < 2$). In the experimental results as described here, the ELMy regime was obtained with plasma current (I_p) around 900 kA, and magnetic field at 5.4 T. Below, we present recent observations of the inter-ELM fluctuations for furthering the understanding of the mechanism limiting the pedestal gradient.

Turbulence measurements between ELMs

To better understand the role of fluctuations in the pedestal dynamics, we investigate both local and global fluctuations during the ELM cycle. The main diagnostics used to probe the inter-ELM fluctuations are the phase contrast imaging (PCI) [5], the O-mode reflectometer [4], the gas puff-imaging, and the magnetic probes systems.

Shown in figure 2 is the spectrogram of the fluctuations between ELMs as measured using the PCI system. Characteristic inter-ELM fluctuations near 300 kHz are clearly observed to onset and last until the next ELM.

Since the PCI measurements are line-integrated sampling both edge and core fluctuations, radial localization of the turbulence remains unclear. However, with the 32 radial chords, a spatial Fourier transform is obtained. Figure 3 displays the spectrum $S(k_R, f)$ as a function of frequency and major radius wavenumber. Beside the broadband fluctuations in this figure, two coherent peaks at $k_R = \pm 1.5 \pm 0.5$ cm^{-1} are observed from which a phase velocity (ω/k) of ± 12 km/s is determined. From the Doppler shift determined from the charge exchange spectroscopy(not shown here), this phase velocity suggests the turbulence is edge localized.

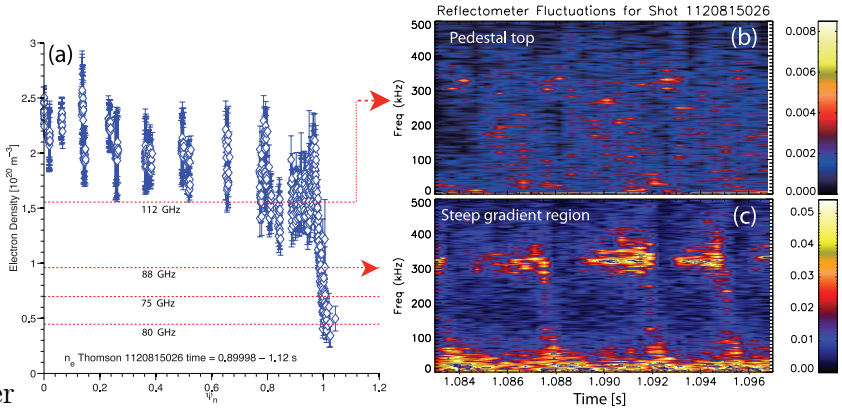

Figure 4: (a) Density profile with reflectometer cutoffs. (b) Spectrogram of the fluctuations as measured by the reflectometer at the pedestal top and (c) in the steep gradient region.

To improve on the radial localization, we used the O-mode multi-channel fixed reflectometer system to probe the edge electron density fluctuations. Figure 4(a) shows the fixed frequency with associated density cutoff layers. While the absolute density fluctuation level was difficult to assess in this experiment, the complex signals from each channel sampling the edge density provide measurements of the fluctuation characteristics at corresponding radii. Figure 4(b)-(c) displays the spectrogram of the complex signals between ELMs. It is observed that the channel probing the steep density gradient exhibits coherent fluctuations that onset after the ELM crashes. The channel probing the pedestal top, on the other hand, does not display any spectral features. This suggests for the time window presented, that the channel either probes further away from the pedestal or the fluctuations are localized in the steep gradient region. The latter is confirm when the overall density is increased to show that pedestal top detect the fluctuations. Overall, the reflectometer results suggest that the coherent fluctuations are localized in the pedestal region.

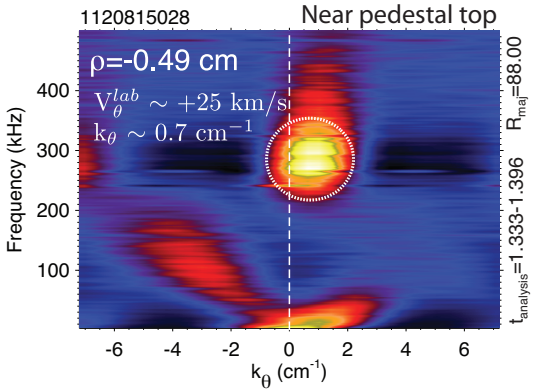

Figure 5: Conditional spectrum $S(k_\theta|f)$ for ρ = -0.49 cm from the separatrix.

The 2D measurements of the edge fluctuations are performed using the HeI gas-puff imaging system [6]. The GPI views the low-field side spanning a 2D cross-section area

of 3.5 cm (radial) by 3.9 cm (poloidal). The collected HeI emission ($\lambda = 587.6$ nm) is detected using an array of avalanche photodiodes sampled at 2 MHz. Figure 5 shows the density fluctuation measurements represented as the conditional spectrum ($S(k_\theta|f)$) for $\rho = -0.49$ cm from the separatrix. These spectra exhibit a coherent fluctuation at 300 kHz peaking at $k_\theta = 0.7$ cm^{-1}, propagating in the electron diamagnetic direction in the laboratory frame.

Another important characterization of the edge fluctuations is its magnetic signature. Such characterization is performed using a double-head magnetic probe dwelled 2 cm from separatrix. The two magnetic heads are separated poloidally by 5 mm enabling the resolution of the poloidal wavenumber spectrum(see probe details in Ref. [7]). Figure 6 displays the inter-ELM magnetic $\tilde{B}_\theta$ fluctuations showing in panel (b) the onset of the coherent fluctuations. This is further highlighted in panel(c) when the integrated power over the frequency band (200 and 500 kHz) shows an increase followed by a saturation of the integrated power. Combined with panel (d), which shows the pedestal electron temperature as measured using the ECE, we observed an increase of the edge temperature followed by the onset of the mode (see panel (c)). Once this mode onsets, the edge temperature saturates until the next ELM. During the inter-ELM phase, a slight increase of the line-integrated density (panel (e)) is observed suggesting that the electron density does not provide the threshold for the onset of the mode. Combining density and temperature at the pedestal, the inter-ELM fluctuations are presented in terms of the electron β at the pedestal in panel figure 6(f) suggesting a β limit as expected for the KBM instability.

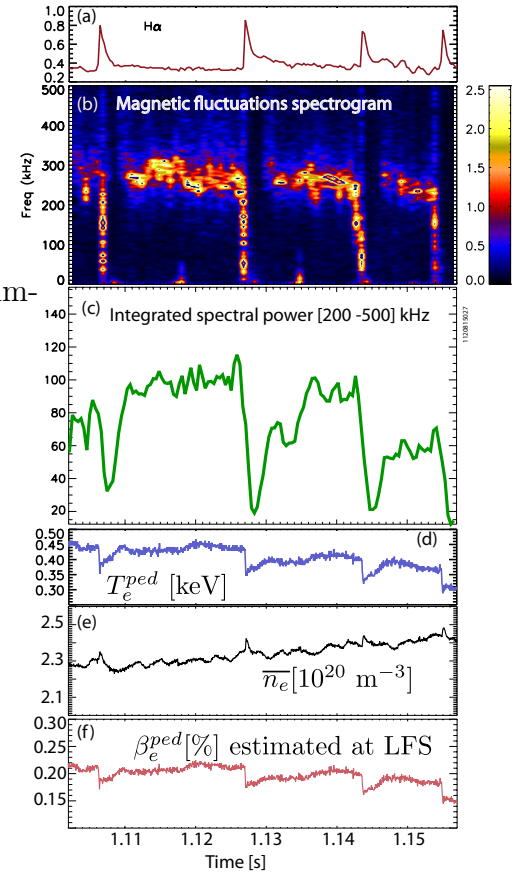

Figure 6: (a) H_α trace indicating the ELMs. (b) Magnetic spectogram. (c) Integrated spectral power of (b). (c) Edge T_e as measured by the ECE radiometer. (e) Line-average density. (f) Estimated β_e at the LCFS.

References

[1] P. B. Snyder, *et al. Phys. Plasmas*, 16:056118, 2009.
[2] S. J. Wukitch, *et al. Physics of Plasmas*, 12(5):056104, 2005.
[3] J.W. Hughes, *et al. Nuclear Fusion*, 53(4):043016, 2013.
[4] A. Dominguez. PhD thesis, MIT, 2012.
[5] Y. Lin, *et al. Review of Scientific Instruments*, 70(1):1078–1081, 1999.
[6] I. Cziegler, *et al. Phys. of Plasmas*, 17, 56120, 2010.
[7] J A Snipes, *et al. Phys. Plasmas*, 16:056118, 2009.